Reliability Evaluation of Novel Core-in-Sheath-Type Carbon/Glass Hybrid Thermoplastic Composite Rods

by

Kimiyoshi NAITO, Hiroyuki OGUMA, Jonathon TANKS, and Chiemi NAGAI
(Research Center for Structural Materials, National Institute for Materials Science, Sengen, Tsukuba, Ibaraki, Japan)

Abstract

In the Center of Innovation science and technology based radical innovation and entrepreneurship (COI STREAM) program, “construction of next-generation infrastructure using innovative materials ~realization of safe and secure society that can coexist with the earth for centuries~”, we focus on the reliability evaluation of the novel core-in-sheath-type carbon/glass hybrid thermoplastic composite rods (hybrid rods). It is necessary to characterize the mechanical properties of FRP because the cables in the infrastructures are usually used in a rope configuration. We also investigated the tensile properties of the hybrid ropes consisting of seven hexagonally close-packed twisted rods with two layers under static and fatigue loadings. The static and fatigue properties of the hybrid ropes can be estimated using a single hybrid rod. Therefore, we showed the various evaluation results for the single hybrid rods in this paper. The morphologies (including constituent volume fractions) of the hybrid rods were characterized by optical and gravimetric methods, and the tensile, axial and transverse compressive, and flexural tests of the hybrid rods under static and fatigue loadings were performed. In addition, interfacial mechanical properties between the carbon fiber bundle core and glass fiber bundles were investigated. Moreover, data accumulation and statistical analyses have been conducted to evaluate the effects of environmental factors, such as temperature, water, and ultraviolet irradiation, on their static properties.

(Received November 15, 2022)

Key Words: carbon fiber, glass fiber, thermoplastic epoxy, hybrid rod, mechanical property, static, fatigue, statistical.

1. Introduction

Tendons are widely used as tension members for civil infrastructure, buildings, and offshore engineering structures. In civil infrastructure and buildings, prestressed concrete is the main material used for beams and floors of bridges (for automobiles and trains) and piers, floors in high-rise buildings, and cylindrical walls and spherical shells in pressure vessels. Tendons are also used for cables in suspension bridges, ground anchors, and repaired/reinforced buildings [1-3]. For offshore structures, prestressed concrete is the main material used in fixed and floating concrete platforms [4-9]. Each tendon is pretensioned, such that it does not slack despite variations in the extreme ocean environment. The tension in the tendons is a function of the environmental conditions under which the structure must operate.

Traditional reinforced concrete uses high-tensile strength steel wires, bars, and rebars. Corrosion and fatigue of steel cables and classical steel reinforcing bars are serious issues [10-12]. Therefore, the use of fiber-reinforced polymer matrix composites (fiber-reinforced plastics, FRP), particularly carbon FRP (CFRP) have been proposed [13-16]. The application of CFRP in construction, particularly in post-strengthening and rehabilitation, is well known and highly appreciated in most applications due to its long-term reliability.

Epoxy resins are frequently used as a matrix in CFRP because they have excellent mechanical properties and good handling properties, including fabrication. Currently, thermosetting epoxy resins are most often used for CFRP tendons [17,18]. However, the inherently brittle nature of epoxy and other thermosetting polymers and their poor resistance to crack initiation and growth are important issues that largely limit their application in certain fields. Epoxy resins are also generally neither fusible nor soluble after curing due to the presence of cross-links in the chemical structure of cured resin. This property significantly restricts the possibility of post-forming, recycling, or reusing.

In contrast, thermoplastic-based CFRPs (CFRTP) have great potential to be post-formed, recycled, and reused because thermoplastic resins are toughened and fusible. However, the manufacturing of CFRTPs usually requires higher energy because high temperatures and pressures are necessary for the impregnation process due to their high molecular weight [19]. A new resin that has both good workability of thermosetting and post-formability, recyclability, or reusability, has been desired for use as the CFRTP matrix.

A new thermoplastic epoxy resin has been recently developed by Nagase ChemteX [20,21], and novel carbon/glass hybrid thermoplastic composite rods called ‘‘CABKOMA” have been developed by Komatsu Matere [22]. The hybrid rods are the core-in-sheath type and consist of a bundle (or bundles) of carbon fiber surrounded by an outer braided bundle glass fiber in which a new thermoplastic epoxy resin is evenly impregnated as a matrix. The new thermoplastic epoxy resin remains thermoplastic even after curing.

In the Center of Innovation science and technology based radical innovation and entrepreneurship (COI STREAM) program, “construction of next-generation infrastructure using innovative materials ~realization of safe and secure society that can coexist with the earth for centuries~”, we focus on the reliability evaluation of the hybrid rods.

The morphology and mechanical properties of the hybrid rods under static and fatigue loadings were evaluated [23-32]. The longitudinal and cross-sectional morphology of the hybrid rods were observed. The volume fraction of carbon fiber, glass fiber, matrix, and void for the rods were estimated using a specific gravity measurement via ethanol immersion and a thermogravimetric analysis. Tensile, axial, and transverse compressive, and flexural tests of the hybrid rods under static and fatigue loadings were performed. In addition, interfacial mechanical properties between the carbon fiber bundle core and glass fiber bundles were investigated. Moreover, data accumulation and statistical analyses have been conducted to evaluate the effects of environmental factors, such as temperature, water, and ultraviolet irradiation, on their static properties. The details of testing results and discussion can be obtained from our published papers [23-32].

We show the advantages and disadvantages of mechanical properties, especially reliabilities, of the hybrid rods in the present study, and as a result, hope that we can obtain the design guidelines for structural factors according to the various application.

2. Experimental Procedures

2.1 Materials

The novel carbon/glass hybrid thermoplastic composite rods have been developed by the Komatsu Matere. Three types of hybrid rods, described as 24K1P, 24K2P, and 24K3P, with differing carbon/glass ratios were fabricated. The hybrid rods are the core-sheath type, fabricated by inserting a carbon fiber bundle (core) into a braided glass fiber tube (sheath), into which the thermoplastic epoxy was evenly infiltrated. The unidirectional carbon fiber core was made of 24k-filament T700SC polyacrylonitrile (PAN)-based carbon fiber (T700SC-24000-50C, Toray) bundles [33], having a filament diameter of $d_f = 6.87$ μm; 24K1P contains one bundle (24,000 filaments), 24K2P contains two bundles (48,000 filaments), and 24K3P contains three bundles (72,000 filaments). The glass fiber sheath was made of 400-filament E-glass fiber (ECG751/01ZY-95T, Z-twist at 1 turn per inch, supplied from Nippon Electric Glass) bundles, having a filament diameter of $d_f = 9.20$ μm; 16 yarns containing three twisted bundles (1,200 filaments, 3.5 turns/inch) each were braided using a maypole braider (fabricated by Taniguchi Seichu). The thermoplastic epoxy in the hybrid rods was made of difunctional epoxy resin and difunctional phenolic compound mixed at a stoichiometric ratio (XNR6850V/XNH6850V = 100/6.5) (Nagase ChemteX) [20,21]. Dry hybrid rods were immersed in methyl ethyl ketone (MEK) solvent solution of the thermoplastic epoxy and then dried in an oven at 150 °C.

2.2 Characterization

The diameters of the hybrid rod were measured using a micrometer. The longitudinal morphology (in plain view) was observed using a digital microscope (VHX-5000 and VH-ZST, Keyence). The rods were cut into roughly 10-mm-long segments using a rotary cutting machine. The specimen for transverse sectional view was embedded in an epoxy resin molding material and then cut and polished on the transverse section. The cross-sectional morphology of the hybrid rods was also observed using a digital microscope (VHX-5000 and VH-ZST, Keyence).

The densities of the hybrid rods (≈ 50 mm long) were measured via ethanol immersion (ASTM D792) [34]. The densities of carbon fiber, glass fiber, and matrix are 1.80 g/cm^3, 2.54 g/cm^3, and 1.20 g/cm^3, respectively. At least 3 specimens were tested for each type of hybrid rod.

Thermogravimetric analysis (TGA) of the hybrid rods (about 5 mm long) was performed at 30–1000 °C at a heating rate of 10 °C/min under atmospheres of N_2 (400 mL/min), Ar (400 mL/min), and N_2/O_2 (4:1) (400/100 mL/min) using a simultaneous thermogravimetric analyzer (STA7300, Hitachi High-Tech Science). At least three specimens were tested for each type of hybrid rod under each condition.

Thermomechanical properties were measured by dynamic mechanical analyzer (DMA7100, Hitachi High-Tech Science) in bending mode, at a frequency of 1 Hz and over a temperature range of −120 °C to 120 °C. The storage modulus (E'), loss modulus (E''), and loss tangent ($\tan(\delta)$) were recorded for each size of hybrid rod.

2.3 Mechanical testing

2.3.1 Static loading

The hybrids rods were trimmed to 250 (190) mm for 24K1P, 350 (250) mm for 24K2P, and 450 (310) mm for 24K3P. The glass fabric/epoxy composite tabs were fabricated using the wet hand layup process to each end of the specimen and a gauge length of 110 (50) mm [35]. The long and short lengths specimens were prepared and () indicated the short length specimen. The specimen was set up on the testing machine using an active gripping system. At least ten replicate specimens were tested at a crosshead speed of 1 mm/min, at the following temperatures: −50 °C, 0 °C, 23 °C, 50 °C, and 80 °C (±3 °C). Temperature was controlled by a small thermostatic chamber, which was placed only around the center of the specimen, such that the grip area was not affected.

To investigate the weathering effect on the tensile strength, the xenon arc lamp accelerated weathering test machine (SX75, Suga Test Instruments) was used for 24K1P sample. A combination of quartz glass and long-pass filters cut wavelengths below 295 nm, with a maximum irradiance of 180 W/m^2 (monitored over 300–400 nm. Temperature and relative humidity were kept constant at 37 °C and 50 %, respectively. The weathering times were set for 335, 1000, 2000, and 3000 h.

The hybrid rods were cut to 60 mm in length; then, glass fabric/epoxy-composite wrapping was applied by the wet hand layup method at each end of the specimens using a gage length of 10 mm [35]. The specimens were fixed to the testing machine using a hydraulic chuck system. The direct axial compressive tests were performed using an electro-servo hydraulic testing machine (MTS858 Mini Bionix, MTS) with a load cell of 25 kN. A crosshead speed of 0.1 mm/min was applied. All the tests were conducted in an ambient environment (temperature of 23±3 °C and 50±5 % relative humidity). Ten specimens were tested all together.

The transverse compressive specimens perpendicular to the rod axis were prepared using a conventional cutting machine via a diamond braided to thicknesses of 5 mm, and the cut surfaces of the specimens were polished. The transverse compressive tests for the hybrid rod were performed through in situ observation using a digital microscope (VHX-5000 and VH-ZST, Keyence) with a compression module system (5 kN load cell, Kammrath & Weiss GmbH). Specimens were placed on a block indenter. The displacement was applied quasi-statically at a crosshead speed of 1.0 μm/sec to obtain the transverse compressive properties of the hybrid rods. In addition, the displacement after a predetermined amount of load was halted to allow the in-situ digital microscope observation of the deformation. All tests were conducted in the laboratory environment at room temperature (at 23±3 °C and relative humidity of 50±5 %). Ten specimens were tested (continuous load condition: Five specimens, predetermined load condition: Five specimens).

Flexural tests were conducted on 50 mm-long rods in four-point bending based on ASTM D6272 [36], with a universal testing machine (Autograph AG-series, Shimadzu) at room temperature (23±3 °C, 50±5 % RH), using a crosshead speed of 1 mm/min. Ten replicate specimens were tested.

The push-out specimens perpendicular to the rod axis were prepared using a conventional cutting machine via a diamond braided to thicknesses of 1.5, 2.0, and 2.5 mm, and the cut surfaces of the specimens were polished. The average diameter of the core is approximately 1.21, 1.80, and 2.13 mm for 24K1P, 24K2P, and 24K3P, respectively. The push-out test was performed on a universal testing machine EZ-Test (Shimadzu) with a load cell of 500 N. To investigate the temperature effect on the interfacial strength, a Peltier heating and cooling system (water cooling type copper Peltier unit PU-50W, switched-mode power supply Z20-10-J, temperature controller SA100, Chiller MP-250B, Takagi Mfg.) was incorporated into the experimental setup. The push-out tests were performed at different temperatures (−20, 0, 23, 35, 50, and 80 °C) after stabilizing the thermal drift with a hold time of 10 min. N_2 gas was introduced to prevent significant condensation on the sample surface when lowering the temperature. To investigate the effect of water absorption on the interfacial mechanical properties, the samples were first immersed in water at room temperature for 24, 72, and 240 h; then, they were placed on the support and tested immediately at 23 °C. Moreover, the samples immersed in water for 240 h were dried with two methods (at 50 °C, under laboratory atmosphere in a hotplate or under vacuum in a vacuum oven) before being tested.

2.3.2 Fatigue loading

Uniaxial fatigue tests were performed under sinusoidal waveform loading by electro-servo-hydraulic testing machines (Servopulser EHF-E, Shimadzu and 858 Mini Bionix, MTS) at 10 Hz. To investigate the effect of test frequency on the fatigue properties, the surface temperature of the samples was separately measured with a thermocouple for test frequencies of 1 and 10 Hz. The stress ratio (ratio of minimum stress to maximum stress in one load cycle) was 0.1, which means that the materials were under tension–tension loading. The tests were terminated after 10^7 cycles. All the tests were conducted in a laboratory environment at room temperature (23±3 °C, 50±5%RH). For the fatigue test, the wet hand layup process was utilized to fabricate the gripping parts of the samples. The gauge length of the fatigue samples was 50 mm, and the samples broke in the gauge section. Strain was measured at the gauge section in the longitudinal direction with strain gauges to detect the stiffness changes that occurred during the test.

The hybrid rods were trimmed to 110 mm. The polyacetal (POM) cone and pillar tube tabs were applied to each end of the specimen. The fatigue flexural tests were performed by complete reversed bending test based on JIS K7082 [37], at room temperature (at 23±3 °C and 50±5% relative humidity), using an electro-servo-hydraulic testing machine (Servopulser EHF-ED20KN-10L, Shimadzu) with a 200 N load cell (LU-20KA, Kyowa). A sinusoidal waveform was applied at a frequency of 1 or 2 Hz with constant amplitude. The stress ratio, R, of the minimum stress to the maximum stress was −1. The tests were terminated after 1×10^7.

3. Results and Discussion

3.1 Physical properties [23,24]

The average diameters of the hybrid rods are summarized in Table I.

Typical longitudinal images of the hybrids rods clearly show that the glass fibers in the hybrid rods are of a braid structure (Fig.1). The biaxial construction has two sets of yarns running in opposite directions, where yarns in one direction are passing under and over the other. The braid angle is the orientation angle of the interlacing yarns with respect to the braid axis. The braid angles of the hybrid rods were measured by taking their image under the digital microscope. The braid angles of hybrid rods are summarized in Table I. Typical cross-sectional images of the hybrids rods clearly show that the individual carbon and glass fibers are well dispersed in the thermoplastic epoxy matrix (Fig.1). Some partial voids were observed at four sites at the boundary between the carbon fiber and glass fiber components as shown in Figs.1(b), (d), and (f) using the arrows.

The densities of the hybrid rods as measured via ethanol immersion are summarized in Table I. TGA was employed to estimate the weight fraction of the hybrid rods. The volume fraction of carbon fiber (V_{CF}), glass fiber (V_{GF}), matrix (V_M), and void (V_V) in each type of hybrid rod (Table I) was calculated based on ASTM D2734 [38].

The glass transition temperature (T_g) was estimated from the initiation point of softening (ie, the first inflection point) in the storage, loss modulus, and loss tangent curve (E', E'', and $\tan(\delta)$ vs temperature). It should be noted that this T_g value is inherently lower compared to calculations using E'' or $\tan(\delta)$ peaks, which are related more to the segmental motion of neat polymers and represents the midway point between glassy and rubbery behavior; however, the E' method is commonly used when mechanical failure is of primary interest [39]. The T_g (onset of E') values are listed in Table I.

3.2 Static test

3.2.1 Tensile properties [23-26]

No difference was observed in the tensile properties for the long and short lengths specimens. For all types of hybrid rods at room temperature or below, the stress applied to the specimen was linearly proportional to the strain until failure. However, at higher temperatures (50 °C and 80 °C), the rods showed some nonlinear behavior near failure (~2.5 % strain), particularly in the case of 80 °C.

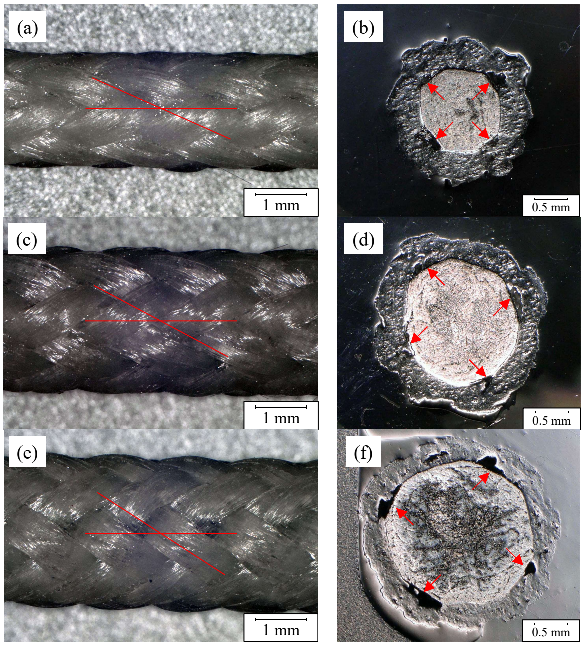

Fig.1 Typical longitudinal and cross-sectional images of the (a, b) 24K1P, (c, d) 24K2P, and (e, f) 24K3P hybrid rods

Table I Physical properties of the hybrid rods

	24K1P	24K2P	24K3P
Diameter d (mm)	2.30	2.73	3.09
Braid angle θ (°)	22.3	30.2	35.2
Density ρ (g/cm^3)	1.759	1.737	1.698
Volume fraction of carbon fiber V_{CF} (%)	24.58	38.34	46.18
Volume fraction of glass fiber V_{GF} (%)	39.75	29.63	23.15
Volume fraction of matrix V_M (%)	25.49	24.54	23.39
Volume fraction of void V_V (%)	10.18	7.49	7.28
Glass transition temperature T_g (°C)	78.6	81.5	77.0

Considering the DMA results, it can be concluded that the tensile behavior of the rods depends on the test temperature relative to the T_g, rather than just the absolute temperature. The tensile modulus was calculated using a least square method for the linear section of tensile stress-strain curve. The average tensile modulus (E), tensile strength (σ_{ult}), and failure strain (ε_{ult}) of the hybrid rods are summarized in Table II. The hybrid rods show carbon-fiber-dominated behavior of the tensile properties in the longitudinal direction of the fiber reinforcements.

As expected, these tensile properties are higher when a higher V_{CF} is used (and thus higher total fiber volume content (V_F)). Although the E and ε_{ult} only show slight downward trend once the temperature nears T_g, σ_{ult} exhibits more temperature sensitivity with a 15% increase at −50 °C compared to room temperature (RT), and a 15% decrease at 80 °C compared to RT (i.e., 30% difference between the two extremes).

When appreciable scattering of tensile strengths is observed, the statistical distribution of fiber and composite strengths is usually described using the Weibull equation [40]. The Weibull modulus values (*m*) for the hybrid rods—summarized in Table II—fall in the range of 15 to 35, while it is typically less than 10 for single carbon fibers [41] and less than 30 for unidirectional CFRP [42]. The *m* for the hybrid rods is higher than for single carbon fibers and is similar to that of unidirectional CFRP.

Table II Tensile properties of the hybrid rods

	Temp. (°C)	24K1P	24K2P	24K3P
Tensile modulus *E* (GPa)	-50	68.1	88.7	98.4
	0	68.9	88.5	97.2
	23	64.7	82.3	100.0
	50	64.6	88.3	98.9
	80	61.8	82.6	93.7
Tensile strength σ_{ult} (GPa)	-50	1.575	2.080	2.297
	0	1.429	1.925	2.118
	23	1.422	1.804	1.998
	50	1.261	1.714	1.944
	80	1.112	1.506	1.687
Failure strain ε_{ult} (%)	-50	2.175	2.131	2.169
	0	2.118	2.148	2.141
	23	2.191	2.045	2.116
	50	2.087	2.087	2.082
	80	2.010	2.043	2.016
Weibull modulus *m*	-50	26.45	31.31	34.74
	0	25.97	30.60	33.39
	23	23.70	26.86	29.91
	50	20.42	23.40	26.58
	80	15.54	18.65	21.55

The V_{CF} of the 24K1P hybrid rod was lowest among the other hybrid rods and the V_V of the 24K1P hybrid rod was quite high. The strength differences between the samples strongly affected the V_{CF} and the void distribution. Therefore, the strength distribution for the 24K1P hybrid rod varied from lower to higher stress levels. Consequently, the *m* of the 24K1P hybrid rod was lower. In contrast, the V_{CF} of the 24K2P hybrid rod was intermediate and the V_{CF} of the 24K3P hybrid rod was highest among the hybrid rods. In addition, the V_V of the 24K2P and 24K3P hybrid rods was intermediate in value and the excess strength affected the V_{CF} and void distribution. Therefore, the strength distributions of the 24K2P and 24K3P hybrid rods were narrow. Consequently, the *m* of the 24K2P and 24K3P hybrid rods were higher.

It also shows a linear relationship with tensile strength for all temperatures and hybrid V_F. This further supports the conclusions, in which the lower temperature leads to brittle fracture and less variable strength (higher Weibull modulus), while higher temperature results in a mixture of fiber rupture and pullout with more variable strength (lower Weibull modulus). The relationship between Weibull modulus and temperature, in which a plateau is visible for temperatures below 0 °C. This may indicate the influence of a single dominant failure mode at low temperatures (brittle fiber rupture), which is the maximum limiting strength of the composite. As temperature increases, the failure mode becomes mixed - including fiber pullout due to a softened matrix - and the Weibull modulus decreases linearly. Differences in the Weibull modulus may also be influenced by the distribution of defects—including void, fiber breakage, and fiber misalignment [43]—introduced during manufacturing and subsequent treatment.

Visible color change was observed after just 300 h of exposure, growing increasingly yellow as time increased (Fig.2). This is a common phenomenon associated with oxidation of phenolic substances, as indicated by the absorbance shift to longer wavelengths after exposure [44,45].

The tensile behavior of the hybrid rods after UV exposure was investigated, revealing linear elastic behavior up to failure for all specimens, which is expected for fiber-dominant tensile properties. The scatter in tensile strength could be also described by the Weibull equation. It appears that the data sets (tensile modulus, strength, failure strain, and Weibull modulus) for all exposure durations differ little from each other (Table III). It was found that the Weibull modulus value (*m*) after 3000 h of exposure decreased. There were a lot of matrix cracks after UV exposure, and the interfacial strength between the glass fiber and matrix decreased after long-time exposure. They seem that the long-time exposure affected the scatter in tensile strength of the hybrid rods.

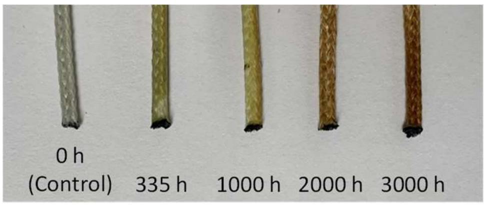

Fig.2 UV-color change over time

Table III Tensile properties of hybrid rods after UV exposure

	Time (h)	24K1P
Tensile modulus *E* (GPa)	0	64.7
	335	67.8
	1000	63.5
	2000	66.4
	3000	66.4
Tensile strength σ_{ult} (GPa)	0	1.421
	335	1.409
	1000	1.423
	2000	1.423
	3000	1.439
Failure strain ε_{ult} (%)	0	2.296
	335	2.108
	1000	2.077
	2000	2.123
	3000	2.332
Weibull modulus *m*	0	25.14
	335	30.67
	1000	28.29
	2000	27.04
	3000	19.98

The static tensile properties of the hybrid rods were also estimated by the rule of mixtures, the laminate theory, and a fiber failure analysis; the calculated results were in good agreement with the test data.

3.2.2 Axial compressive properties [27]

The strain was linearly proportional to the applied stress until failure. The axial compressive moduli of the samples were calculated using the least square method for the straight-line section of the axial compressive stress-strain curve. The average axial compressive modulus (E_C), strength ($\sigma_{C.ult}$), and failure strain ($\varepsilon_{C.ult}$) of the specimens are listed in Table IV.

The E_C and $\sigma_{C.ult}$ increased with an increase in the V_{CF}, whereas the $\varepsilon_{C.ult}$ decreased as the V_{CF} increased. Inversely, the E_C and $\sigma_{C.ult}$ decreased as the V_M increased, whereas the $\varepsilon_{C.ult}$ increased as the V_M increased. The axial compressive properties (modulus, strength, and failure strain) were observed to have linear relationships with the V_{CF} and V_M.

The scatter in axial compressive strength could be described by the Weibull equation [40] and the values for Weibull modulus (m_C) are summarized in Table IV. The m_C increased with increasing $\sigma_{C.ult}$, indicating that the greater the strength of the hybrid rods the narrower the strength distribution. The m_C also increased with increasing V_{CF} and with decreasing V_M and V_V. It exhibits a linear relationship with each of the V_{CF}, V_M, and V_V. The V_{CF} of the 24K1P was the lowest, making the V_M the highest among the other specimens. The variations in the V_{CF}, V_M and void distributions showed a great effect on the strength of the samples.

Table IV Axial compressive properties of the hybrid rods

	24K1P	24K2P	24K3P
Axial compressive modulus E_C (GPa)	53	78	92
Axial compressive strength $\sigma_{C.ult}$ (GPa)	0.156	0.266	0.271
Failure strain $\varepsilon_{C.ult}$ (%)	0.343	0.325	0.290
Weibull modulus m_C	13.10	15.13	15.60

Thus, the strength distribution for the 24K1P varied from lower to higher stress levels. Consequently, its m_C was the lowest. On the other hand, the V_{CF} and V_M of the 24K2P was intermediate, whereas V_{CF} of the 24K3P was the highest; hence, its V_M was the lowest. Moreover, the V_V of the 24K2P and 24K3P were intermediate. The excess strength affected the V_{CF}, V_M, and void distribution. Thus, the 24K2P and 24K3P exhibited narrower strength distributions compared with that of 24K1P. Consequently, their m_C were high.

3.2.3 Transverse compressive properties [28]

The transverse compressive load per unit length (F)-displacement (U) curves showed large nonlinear behavior and complicated shape. In the initial stage, the load gradually increased by increasing the deformation. This behavior was caused by the increase in the contact zone. In the second stage, the load-displacement relation was fitted by the analytical relation (stable deformation region). Subsequently, the slope dF/dU decreased slightly. Finally, the load-displacement curve showed a clear increase in slope dF/dU as the deformation proceeded. The transverse compressive modulus (E_{TC}) was calculated from the F-U curve using the least square fitting method for the analytical relation. The transverse compressive stress at which these tangent lines intersect is defined as the transverse compressive strength (σ_{TC}). The E_{TC} and σ_{TC} are summarized in Table V. The matrix and glass fiber might be reduced the stress in carbon fiber bundle core. The σ_{TC} strongly depended on the matrix and glass fiber volume fraction. The matrix and glass fiber volume fraction of 24K1P were larger than those of 24K2P and 24K3P. The σ_{TC} decreased by increasing V_{CF} (decreasing V_M and V_{GF}), while the E_{TC} were almost similar among these hybrid rods.

Table V Transverse compressive properties of the hybrid rods

	24K1P	24K2P	24K3P
Transverse compressive modulus E_{TC} (GPa)	0.655	0.644	0.639
Transverse compressive strength σ_{TC} (MPa)	15.26	8.79	8.05

3.2.4 Flexural properties [29]

Initially, the stress was linearly proportional to the strain (this modulus was defined as flexural modulus (E_F)). Nonlinear deformation was observed (proportional limit stress ($\sigma_{F.limit}$), limit strain ($\varepsilon_{F.limit}$), and the second slope (0.6 % <strain<0.8 %) was defined as secondary modulus (E_F^*)) subsequently until the stress reached its maximum (the maximum stress was defined as flexural strength ($\sigma_{F.ult}$) and its strain was defined as strain at maximum stress ($\varepsilon_{F.max}$)). Afterward, the stress decreased until fracture of the sample occurred. The differences of nonlinear stresses and secondary modulus observed in the stress-strain curves for three hybrid rods were strongly dependent on the differing carbon/glass ratios. The carbon/glass ratios (V_{CF}/V_{GF}) were 0.62 (24K1P), 1.29 (24K2P), and 1.99 (24K3P), respectively. The volume fraction of glass fiber of 24K1P was highest, and the nonlinear stress and secondary modulus were lowest among the hybrid rods. The E_F, E_F^*, $\sigma_{F.limit}$, $\varepsilon_{F.limit}$, $\sigma_{F.ult}$, and $\varepsilon_{F.max}$ are summarized in Table VI. The E_F, E_F^*, $\sigma_{F.limit}$, and $\sigma_{F.ult}$ were 24K1P<24K2P<24K3P. However, the $\varepsilon_{F.limit}$ and $\varepsilon_{F.max}$ were 24K3P<24K2P<24K1P.

Table VI Flexural properties of the hybrid rods

	24K1P	24K2P	24K3P
Flexural modulus E_F (GPa)	33	47	57
Secondary modulus E_F^* (GPa)	22	37	47
Limit stress $\sigma_{F.limit}$ (GPa)	0.174	0.241	0.275
Limit strain $\varepsilon_{F.limit}$ (%)	0.542	0.473	0.462
Flexural strength $\sigma_{F.ult}$ (GPa)	0.264	0.362	0.377
Strain at max. stress $\varepsilon_{F.max}$ (%)	1.102	1.013	0.988
Weibull modulus m_F	12.36	15.71	17.93

The strength ($\sigma_{F.limit}$ and $\sigma_{F.ult}$) and modulus (E_F and E_F^*) increased with the V_{CF}, whereas the strain ($\varepsilon_{F.limit}$ and $\varepsilon_{F.max}$) decreased. In contrast, the strength ($\sigma_{F.limit}$ and $\sigma_{F.ult}$) and modulus (E_F and E_F^*) decreased with an increase in V_M and V_V. The strain ($\varepsilon_{F.limit}$ and $\varepsilon_{F.max}$) increased with an increase in V_M and V_V.

The scatter in flexural strength could be described by the Weibull equation [40] and the values for Weibull modulus (m_F) are summarized in Table VI. The Weibull modulus increased with increasing flexural strength for the hybrid rods, indicating that the greater strength of the hybrid rods caused a narrower strength distribution. The Weibull modulus increased with increasing V_{CF}, and decreasing V_M and V_V of the hybrid rods.

The m_F was lower than m and was similar to m_C. The internal fracture (fracture of carbon fiber bundle core) of the hybrid rods was observed in the longitudinal direction. Cracks propagated through kinking of the aligned tows, localized buckling, and matrix cracking (delamination or splitting). Such kinking, localized buckling, and matrix cracking behavior of unidirectional carbon fiber bundle composites in the hybrid rods affected the static flexural properties. The macroscopic failure modes of the hybrid rods under static flexural loading were buckling in the compressive side. Static flexural properties strongly depended on the axial compressive properties of the hybrid rods. The 24K1P hybrid rod has the lowest V_{CF}, and the highest V_M and V_V, all of which significantly contribute to the strength differences between samples. Therefore, the strength distribution for the 24K1P hybrid rod varied widely, resulting in a lower Weibull modulus. By contrast, V_{CF} was highest for 24K3P and V_M was lowest, while the values for 24K2P were between 24K1P and 24K3P. In addition, V_V of the 24K2P and 24K3P specimens, while not significantly lower, was intermediate in value and was considered to influence the higher observed strength, along with V_{CF} and V_M. Therefore, it follows that the narrower strength distributions of the 24K2P and 24K3P hybrid rods would correspond to higher values of the Weibull modulus. It was found that the m_F improved with increasing the V_{CF}, decreasing the V_M and V_V.

3.2.5 Interfacial shear properties [30,31]

Fig.3 shows the schematic of the push-out test.

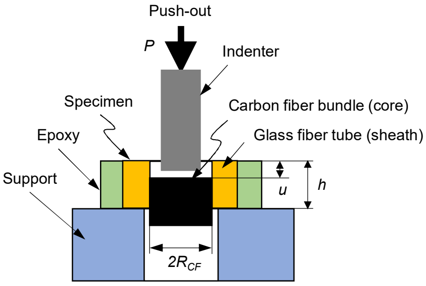

Fig.3 Schematic of the push-out test

The interfacial shear sliding stress for the displacement of a carbon fiber bundle core, τ_s, after the onset of the debonding was obtained from the push-out test.

$$\tau_s = \frac{P}{2\pi R_{CF}(h-u)} \tag{1}$$

where P is the load measured at the displacement, u, of the carbon fiber bundle core, h is thickness of specimens, and R_{CF} is the average radius of the carbon fiber bundle core.

With the increase in the u up to the maximum load (P_{max}), the P exhibited an almost linear increase at first and then gradually decreased. The decrease of the P was supposedly related to the onset of interfacial debonding. The interfacial debonding strength (τ_{ds}) were calculated by substituting u with 0, and P with the P_{max} in Eq. 1. After the onset of debonding, the P–u curve exhibited sinusoidal behavior during the sliding process. The interfacial shear sliding strength (τ_{ss}) calculated by the average of τ_s.

The macroscopic observations after the removal of the glass fiber bundles for the hybrid rods were examined. The bonding and non-bonding areas of the braided glass fiber bundles were clearly distinguished. The measured bonding area ratios of the glass fiber bundles were 0.807, 0.575, and 0.615 for the 1P, 2P, and 3P hybrid rods, respectively. With the increase in the bonding area, τ_{ds} and τ_{ss} increased; their values τ_{ds}, τ_{ss}, and variations are assumed to be associated with the bonding area and shape, as well as the dimensions of the non-bonding area.

The actual debonding strength ($\tau_{ds.act}$) and actual sliding strength ($\tau_{ss.act}$) were calculated using the bonding area ratio. The $\tau_{ds.act}$ and $\tau_{ss.act}$ are summarized in Table VII.

The $\tau_{ds.act}$ and $\tau_{ss.act}$ decreased with increasing the temperature for all the three hybrid rods. However, all the samples exhibited similar $\tau_{ds.act}$ and $\tau_{ss.act}$ values at the same temperature, while large scattering was observed. The temperature dependence of the interfacial shear properties could be estimated via DMA tests at different temperatures. Similar discussion was found by the decrease in shear transfer between fibers as the polymer matrix grows softer, which could be correlated between different temperatures by DMA measurements of the storage modulus [46].

Table VII Interfacial shear properties of the hybrid rods

	Temp. (°C)	24K1P	24K2P	24K3P
Actual debonding strength $\tau_{ds.act}$ (MPa)	-20	35.67	24.82	28.82
	0	30.28	22.19	26.49
	23	24.40	19.69	22.30
	35	19.05	15.28	17.71
	50	13.60	11.99	14.76
	80	8.60	9.64	10.38
Actual sliding strength $\tau_{ss.act}$ (MPa)	-20	17.24	10.27	13.18
	0	11.88	9.45	11.75
	23	7.12	6.06	7.68
	35	3.40	5.62	5.33
	50	2.68	5.26	5.97
	80	1.69	2.08	5.19
	Time (h) /dry method	24K1P	24K2P	24K3P
Actual debonding strength $\tau_{ds.act}$ (MPa)	0	24.40	19.69	22.30
	24	22.08	14.32	17.43
	72	21.35	13.35	15.24
	240	13.50	14.74	17.52
	dry (hotplate)	25.83	20.92	20.16
	dry (vacuum)	24.76	19.21	20.76
Actual sliding strength $\tau_{ss.act}$ (MPa)	0	7.12	6.06	7.68
	24	5.26	5.63	6.11
	72	6.12	4.22	5.79
	240	4.01	4.72	5.80
	dry (hotplate)	8.42	7.89	8.39
	dry (vacuum)	7.05	6.78	6.44

The $\tau_{ds.act}$ and $\tau_{ss.act}$ decreased with increasing the water immersion time and then they were both restored after drying for all the samples. However, the three hybrid rods exhibited similar $\tau_{ds.act}$ and $\tau_{ss.act}$ values under the same conditions, while large scattering was observed. The water immersion time dependence of the interfacial shear properties could be estimated using the mass uptake behavior. Water absorbed into a polymer composite by the mechanism of diffusion and other mechanisms were the water transport across the interface or inside microcracks. Similar results and discussion were found in carbon/polyphenylene sulfide [47], glass/polyester [48], and aramid/epoxy composites [49].

3.3 Fatigue test

3.3.1 Tensile properties [25,32]

Fig.4 illustrates the number of cycles to failure (N_f) as a function of maximum stress (σ_{max}) (S–N diagram). The fatigue life at the test frequency of 1 Hz was always within the margin of variation of the results obtained at 10 Hz. The temperatures observed at 10 Hz were higher than those at 1 Hz. The temperature of the sample surfaces reached ~40 and ~35 °C at high-stress ($\sigma_{max} = 0.7\ \sigma_{ult}$) and low-stress conditions ($\sigma_{max} = 0.5\ \sigma_{ult}$). However, there was no close correlation between temperature increment and fatigue life. The temperature dependent mechanical behavior of the hybrid rods were investigated. The tensile, interfacial shear properties, and DMA results showed a dependency of the mechanical behavior on the test temperature depending on the glass transition temperature (~80 °C) rather than just the absolute temperature of all types of hybrid rods types. Therefore, the effect of test frequency on the fatigue properties of the hybrid rods was sufficiently small below 10 Hz. The regression lines of the semi-logarithmic curve (Stromeyer's expression [50]) in Fig.4 were obtained with the method of least squares by using the data from the failure sample as follow:

$$\sigma_{max} = 10^{-Alo\quad {}_{f}+B}+\mathrm{C} \tag{2}$$

The slopes of 24K1P and 24K2P were steep for a short fatigue life and became gradually flatter for longer ones.

The slope of the 24K3P was smaller, indicating that its fatigue life depended more strongly on the applied load than that of the other hybrid rod types. The gentle slope observed in the *S*–*N* diagram was typical of the fatigue test results of carbon fibers and CFRPs [51-53]. The hybridization and existence of voids might have affected the stress dependency of fatigue life in this case, and the gentle slope of 24K3P was probably due to a higher V_{CF} and a lower V_V. To investigate the variation in fatigue strength for a given number of cycles to failure, the regression lines were shifted along the longitudinal axis by two standard deviations of the tensile strength values. Most data were distributed between the lines, indicating that the variations in fatigue strength were comparable to those in tensile strength for each type of rod.

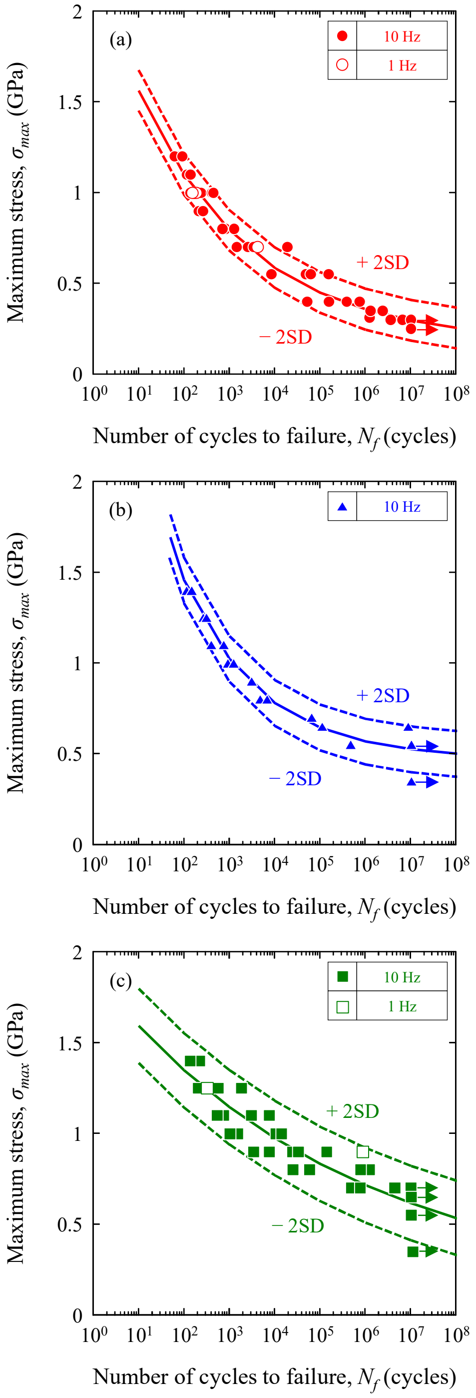

Fig.4 Number of cycles to failure as a function of maximum stress (S–N diagram) for the hybrid rods (a) 24K1P, (b) 24K2P, and (c) 24K3P.

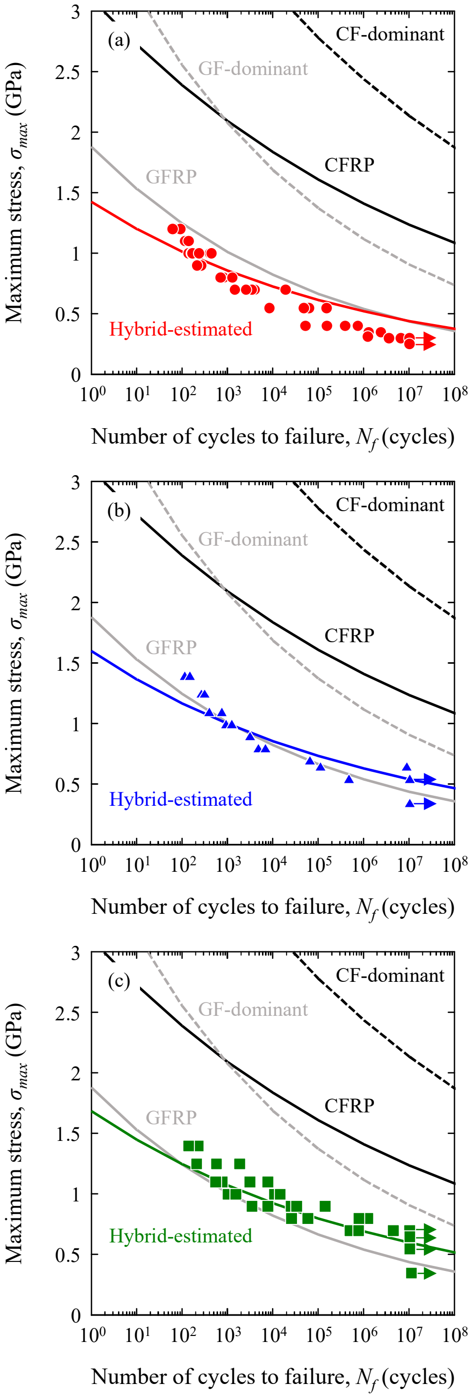

Fig.5 Estimated fatigue tensile behavior of the hybrid rods (a) 24K1P, (b) 24K2P, and (c) 24K3P.

The fatigue strength at 10^7 cycles for 24K1P, 24K2P, and 24K3P were 0.30, 0.53, and 0.62 GPa, respectively, that is, ~21 %, 29 %, and 34 % of their corresponding tensile strengths. In general, the fatigue strength of unidirectional carbon fiber composites with a thermosetting epoxy resin matrix is approximately 50–80 % of the tensile strength [51-53]. This result demonstrates that the fatigue strength of the hybrid rods was lowered by the hybridization in the material.

The fatigue behavior of the hybrid rods was predicted via the rule of mixtures by obtaining fatigue test data on unidirectional CFRP and GFRP (glass-fiber-reinforced plastic) laminated plates made of the same fibers, separately, as the hybrid rods. The results are shown in Fig.5. The estimated lines well illustrated the test data for the higher V_F, that is, the total fraction of carbon and glass fibers. For 24K1P, the estimated lines were mainly located on the higher stress side of the test data when the strength ratio was smaller than 0.7; the presence of voids, which could have served as stress concentration part and fatigue fracture origin, may relate to this tendency. When the strength ratio exceeded 0.7, instead, the test data were located on the higher stress side of the estimated lines. For 24K2P and 24K3P, the estimated lines passed through the data points and expressed the fatigue properties of the hybrid rods. Their higher V_F and lower V_V probably relate to the higher accuracy of this prediction. The *S–N* curves of the hybrid rods in the present study did not show a folding shape. This dependency is probably due to the different structure of materials, that is, laminate and core-in-sheath-type structures. In the core-in-sheath-type hybrid rods, the CFRP and GFRP parts exist inside and outside separately, and their cross-interaction is expected to be smaller than that in a laminate structure with thin layers. This is probably one of the reasons why the *S–N* properties of the hybrid rods could be expressed by those of their constituent fibers and a simple parallel model.

3.3.2 Flexural properties [29]

Fig.6 shows the trend between the maximum flexural stress ($\sigma_{F.max}$) and the number of cycles to failure (N_f), which is alternatively defined as the *S–N* curve for these hybrid rods.

The flexural fatigue properties of 24K3P and 24K2P were higher than those of 24K1P, which correlates to the difference in static strength, i.e., the flexural fatigue performance (in terms of maximum stress) increases with the static flexural strength. The fatigue flexural strengths at 10^7 cycles ($\sigma_{F.th}$) for the 24K2P and 24K3P hybrid rods was higher than that for the 24K1P hybrid rod and the $\sigma_{F.th}$ for the hybrid rods were less than 20% (24K1P), 27% (24K2P), and 30% (24K3P) of the $\sigma_{F.ult}$. Fig.6 also shows the *S–N* curves for the hybrid rods in log–log scale. The power law model [54] is given by,

$$\sigma_{F.max} = A_F\left(N_f\right)^{B_F} \qquad (3)$$

where A_F and B_F are experimental constants. Least squares fitting of the fatigue data exhibited the same trend as a power law model, as illustrated in Fig. 6. The intercept under flexural loading, A_F was 24K1P<24K2P<24K3P and the absolute value of slope under flexural loading, $|B_F|$ was 24K3P<24K2P<24K1P. The A_F increased with increasing V_{CF} and decreasing V_M and V_V of the hybrid rods. A linear relationship was observed between A_F and V_{CF}, V_M, V_V. The $|B_F|$ decreased with increasing V_{CF}, and increasing V_M and V_V of the hybrid rods. There exist linear relationships between the $|B_F|$ and V_{CF}, V_M, V_V. The $\sigma_{F.th}$ increased with increasing V_{CF}, and decreasing V_M and V_V of the hybrid rods. There exist linear relationships between the $\sigma_{F.th}$ and V_{CF}, V_M, V_V.

4. Conclusion

Reliability evaluation of the novel core-in-sheath-type carbon/glass hybrid thermoplastic composite rods (hybrid rods) were investigated. The morphology and mechanical properties of the hybrid rods under static and fatigue loadings were evaluated. The longitudinal and cross-sectional morphology of the hybrid rods were observed. The volume fraction of carbon fiber, glass fiber, matrix, and void for the rods were estimated using a specific gravity measurement via ethanol immersion and a thermogravimetric analysis. Tensile, axial and transverse compressive, and flexural tests of the hybrid rods under static and fatigue loadings were performed. In addition, interfacial mechanical properties between the carbon fiber bundle core and glass fiber bundles were investigated. Moreover, data accumulation and statistical analyses have been conducted to evaluate the effects of environmental factors, such as temperature, water, and ultraviolet irradiation, on their static properties. The results of the hybrid rods are summarized as follows:

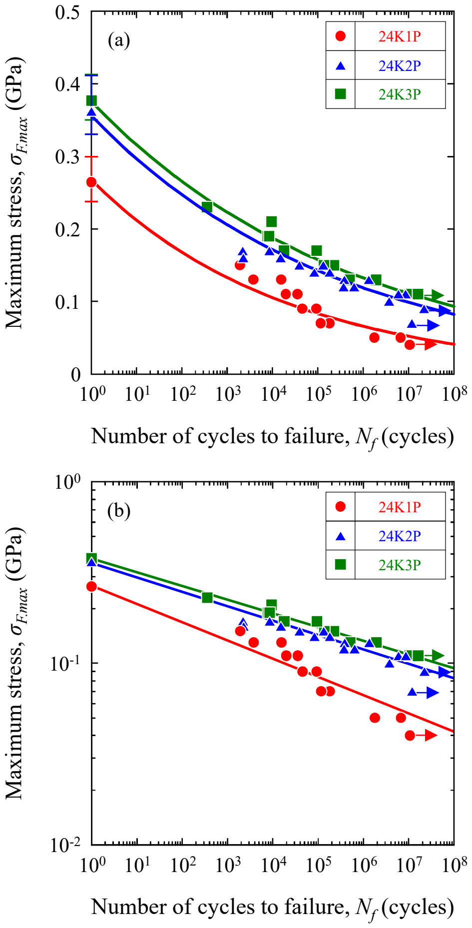

Fig.6 Relation between the maximum flexural stress and the number of cycles to failure, *S–N* diagram for the hybrid rods. (a) *S–N* diagram and (b) *S–N* diagram in log–log scale

The hybrid rods have a braid structure, with various diameters and braid angles. Voids are clearly visible in the cross-sectional view of hybrid rods. The densities, volume fractions of elements (carbon fiber, glass fiber, matrix, and void), and glass transition temperatures were determined.

For static tensile test, the stress applied to the hybrid rods was linearly proportional to the strain until failure for nearly all tested temperatures, with only 80 °C showing slight inelastic deformation near failure due to the softening of the resin matrix. The Weibull modulus was shown to depend on the carbon fiber volume fraction and temperature also has significant influence. This was explained by the relative brittleness of the epoxy matrix as a function of temperature, such that low temperature results in less variable failure stresses and thus higher Weibull modulus, whereas higher temperature leads to a complex mixture of fiber pullout and fiber rupture, yielding variable failure stresses and a lower Weibull modulus. The data sets (tensile modulus, strength, failure strain, and Weibull modulus) for all exposure durations differ little from each other.

For static axial compressive test, the stress applied to the specimen was linearly proportional to the strain until failure. The axial compressive modulus and strength increased with an increase in the volume fraction of the carbon fiber. However, the failure strain decreased as the volume fraction of carbon fiber increased. The Weibull modulus of the hybrid rods increased as the axial compressive strength and carbon fiber volume fraction increased, and void volume fraction decreased.

For static transverse compressive test, the transverse compressive strength decreased by increasing volume fraction of carbon fiber, while the transverse compressive moduli were almost similar among these hybrid rods.

For static flexural test, linear stress–strain behavior was followed by nonlinear deformation as the stress reached its maximum, then the stress decreased rapidly until fracture of the fibers occurred. The flexural modulus, strength, and Weibull modulus increased with carbon fiber volume fraction, which is inverse to the decrease in matrix and void contents. In contrast, the strain at maximum stress decreased as a function of increase in carbon fiber volume fraction, and as a function of decrease in matrix and void contents of the hybrid rods.

For static interfacial shear (push-out) test, the interfacial debonding and sliding strengths decreased with increasing the temperature. The interfacial strengths also decreased with increasing water immersion time, and they were both restored after drying for all the hybrid rods tested. The temperature dependence of the interfacial shear properties of hybrid composite rods could be estimated via dynamic mechanical analysis at different temperatures, while the water immersion time dependence of the interfacial shear properties of hybrid composite rods could be determined using the mass uptake behavior of thermoplastic epoxy.

For fatigue tensile test, the fatigue life was always within the margin of variation and the test frequency effect was negligible for the conditions in the tested materials. The regression lines of the semi-logarithmic curves were in good agreement with the fatigue test data, and the variations in fatigue strength for a given number of cycles to failure were comparable to that in tensile strength for each type of rod. The hybridization and existence of voids strongly affected the stress dependency of the fatigue life. The fatigue behavior of the hybrid rods could be predicted via the rule of mixtures by using fatigue test data of unidirectional CFRP and GFRP laminated plates.

For fatigue flexural test, the intercept for power law model and the fatigue strength at 10^7 cycles increased as a function of increase in carbon fiber volume fraction, and as a function of decrease in matrix and void contents of the hybrid rods. In contrast, the absolute values of slope for power law model decreased as a function of increase in carbon fiber volume fraction, and as a function of decrease in matrix and void contents of the hybrid rods.

Although the hybrid rods used in structures are most often subjected to tensile loading, they occasionally experience compressive, flexural, and shear loadings as well, so these properties must also be characterized. The hybrid (composite) rods had advantages and disadvantages that differed from conventional steel rods. In particular, attention should be paid to low compression and flexural strength, and low operating temperature. We believe that the results in this study will be useful for the handling and design guidelines.

Acknowledgements

This research was promoted by COI program "Construction of next-generation infrastructure using innovative materials ~Realization of safe and secure society that can coexist with the Earth for centuries~" supported by Japan Science and Technology Agency (JST) Grant Number JPMJCE1315.

References

1. Gilbert, R. I. and Mickleborough, N. C., *Design of prestressed concrete*, Spon Press, New York (1990).
2. Nawy, E. G., *Prestressed concreate: a fundamental approach*, Prentice Hall, New York (2009).
3. Soils & Structures No. 222, *The Freyssinet group magazine* (2003).
4. Burnside, O. H. and Pomerening, D. J., Survey of experience using reinforced concrete in floating marine structure. Technical report SSC-321 (1984).
5. *Floating concrete structures - examples from practice, second printing*, VSL International Ltd., Switzerland (1992).
6. Petroleumstilsnet, *Ocean structures*: *Ageing of offshore concrete structures*. Petroleum safety authority Norway, OSL-804-R04-2 (2009).
7. Mangala, M. G. and Haym, B., Journal of Sound and Vibration, 293: 38-58 (2006).
8. Senjanovic, I., Tomic, M., and Rudan, S., Engineering Structures, 56: 117-25 (2013).
9. Zhao, Y., Yang, J., and He, Y., Energies, 5: 3874-3891 (2012).
10. Watson, S. C. and Stafford, D., Civil Engineering-ASCE, 58: 38–41 (1988).
11. Périer, V., Dieng, L., Gaillet, L., Tessier, C., and Fouvry, S., Wear, 267: 308-314 (2009).
12. Hobbs, R. E. and Ghavani, K., International Journal of Fatigue, 4: 69-72 (1982).
13. Balaguru, P., Nanni, A., and Giancaspro, J., *FRP composites for reinforced and prestressed concrete structures: a guide to fundamentals and design for repair and retrofit*, Taylor, New York (2009).
14. Meier, U., Applied Composite Materials, 7: 75-94 (2000).
15. Maissen, A., Structural Engineering International, 7:284-287 (1997).
16. Meier, U., Arabian Journal for Science and Engineering, 37: 399-411 (2012).
17. Burks, B. M., Armentrout, D. L., Baldwin, M., Buckley, J., and Kumosa, M., Composites Science and Technology, 69: 2625-2632 (2009).
18. Barjasteh, E., Bosze, E. J., Tsai, Y. I., and Nutt, S. R., Composites Part A, 40: 2038-2045 (2009).
19. d'Hooghe, E. L. and Edwards, C. M., Advanced Materials, 12: 1865-1868 (2000).
20. Nagase ChemteX Corporation, *Process for Production of Thermoplastic Cured Epoxy Resin with Transparency to Visible Light, and Thermoplastic Epoxy Resin Composition*. United States Patent Application Publication, Pub. No. US2014/0194590 A1 (2014).
21. Imanishi, T., Nishida, H., Hirayama, N., and Tomomitsu, N., ICCM-16 Conference Proceedings, 194-195 (2007).
22. *Komatsu Matere fabric laboratory* [fa-bo], https://www.komatsumatere.co.jp/.
23. Naito, K. and Oguma, H., Composite Structures, 161: 23-31 (2017).
24. Naito, K., Oguma, H., and Nagai, C., Polymer Composites, 41: 3985-3995 (2020).
25. Naito, K. and Oguma, H., Matéria (Rio de Janeiro), 22: e-11843 (2017).
26. Tanks, J. and Naito, K., Journal of Building Engineering, 48: 103922 (2022).
27. Naito, K. and Nagai, C., Journal of Materials Engineering and Performance, 29: 4804-4813 (2020).

28. Naito, K., Nagai, C., and Tanaka, Y., Journal of Physical Science and Application, 9: 25-33 (2019).
29. Naito, K., Applied Composite Materials, 28: 753-766 (2021).
30. Naito, K., Composite Structures, 257: 113129 (2021).
31. Naito, K. and Nagai, C., Composite Structures, 282: 115103 (2022).
32. Oguma, H. and Naito, K. Fatigue and Fracture of Engineering Materials and Structures, 45: 3514-3523 (2022).
33. *High-performance carbon fiber Torayca*, Toray Industries, Inc., https://www.toraycma.com/
34. ASTM D792-13, *Standard Test Methods for Density and Specific Gravity (Relative Density) of Plastics by Displacement*, ASTM International, West Conshohocken, PA (2013).
35. Naito, K., Oguma, H., Hayashi, Y., Nakayama, T., and Noda, H., *Fixing structures of fiber reinforced plastics cables and its fabrication, Strength Testing Methods, and Strength Testing Specimens*, Patent, No. 2015–137928 (Japanese) (2015).
36. ASTM D6272-10, S*tandard test method for flexural properties of unreinforced and reinforced plastics and electrical insulating materials by four-point bending*, ASTM International, West Conshohocken, PA (2010).
37. JIS K7082-1993, *Testing method for complete reversed plane bending fatigue of carbon fibre reinforced plastics*, Japanese Industrial Standards Committee, Tokyo (1993).
38. ASTM D2734-09, *Standard Test Methods for Void Content of Reinforced Plastics*, ASTM International, West Conshohocken, PA (2009).
39. Turi, E. A., *Thermal Characterization of Polymeric Materials*, 2nd ed., Vol. 1, Academic Press, New York (1997).
40. Weibull, W., Journal of Applied Mechanics, 18: 293-297 (1951).
41. Naito, K., Tanaka, Y., Yang, J. M., and Kagawa, Y., Carbon, 46: 189-195 (2008).
42. Naito, K., Yang, J. M., and Kagawa, Y., Journal of Materials Science, 47: 2743-2751 (2012).
43. Qiu, Y. and Schwartz P., Composites Science and Technology, 47: 289-301 (1993).
44. Nikafshar, S., Zabihi, O., Ahmadi, M.,Mirmohseni, A., Taseidifar, M., and Naebe, M., Materials 10: 180 (2017).
45. Malajati, Y., Therias, S., and Gardette, J. L., Polymer Degradation and Stability, 96: 144-150 (2011).
46. Bosze, E. J., Alawar, A., Bertschger, O., Tsai, Y. I., and Nutt, S. R., Composites Science and Technology, 66: 1963-1969 (2006).
47. Batista, N. L., de Faria, M. C. M., Iha, K., de Oliveira, P. C., and Botelho, E. C., Journal of Thermoplastic Composite Materials, 28: 340-356 (2015).
48. Gautier, L., Mortaigne, B., and Bellenger, V., Composites Science and Technology, 59: 2329-2337 (1999).
49. Tanaka, K., Minoshima, K., Grela, W., and Komai, K., Composites Science and Technology, 62: 2169-2177 (2002).
50. Stromeyer, C. E., Proceedings of the Royal Society of London, 90: 411-425 (1914).
51. Kafodya, I., Xian, G., and Li, H., Composites Part B, 70: 138-148 (2015).
52. Shen, C. H. and Springer, G. S., Journal of Composite Materials, 11: 2-16 (1977).
53. Myllläria V., Ruoko, T. P., Vuorinen, J., and Lemmetyinen, H., Polymer Degradation and Stability, 120: 419-426 (2015).
54. Harris, B., *Fatigue in Composites*, Woodhead Publishing, Cambridge (2003).